Catalysis Today xxx (2013) xxx–xxx

Contents lists available at SciVerse ScienceDirect

Catalysis Today

journal homepage: www.elsevier.com/locate/cattod

Co/ZrO_2, Co/CeO_2 and MnCoCe structured catalysts for COPrOx

Leticia E. Gómez, Alicia V. Boix*, Eduardo E. Miró

Instituto de Investigaciones en Catálisis y Petroquímica, INCAPE (CONICET, FIQ-UNL), Santiago del Estero 2829, 3000 Santa Fe, Argentina

ARTICLE INFO

Article history:
Received 4 March 2013
Received in revised form 9 May 2013
Accepted 13 May 2013
Available online xxx

Keywords:
COPrOx
Structured catalysts
Mn
Co_3O_4
CeO_2

ABSTRACT

Cordierite monoliths washcoated with MnCoCe(CP), $Co(I)/ZrO_2$ and $Co(I)/CeO_2$ catalysts were prepared and studied for the CO preferential oxidation (COPrOx) reaction. Among them, the MnCoCe/M system presented the best CO conversion at low temperatures and the $Co(I)/CeO_2$-M catalyst, the best selectivities toward CO_2. In the three catalysts, Co_3O_4 was the main Co containing compound and it was the active species for the COPrOx reaction. Nevertheless, the $Co(I)/CeO_2$-M and MnCoCe/M solids resulted more active than $Co(I)/ZrO_2$-M, possibly due to the better redox properties of the ceria. In the MnCoCe/M catalyst prepared by co-precipitation, the addition of Mn represented an additional positive effect. The presence of Mn promoted the re-oxidation of Co^{2+} to Co^{3+} and, consequently, the activity increased at low temperature. It is also shown that homogeneous and mechanically stable coatings on the walls of the three monolithic catalysts were obtained, which in turn yielded promising results in the COPrOx reaction.

1. Introduction

One way to produce the hydrogen to be used in PEM fuel cells is by means of steam reforming or autothermal reforming of hydrocarbons. Generally, this step is followed by the Water Gas Shift reaction, where the hydrogen stream is purified. However, the effluent of the WGS reaction contains around 1% CO and it could poison the cell anode. The CO preferential oxidation (COPrOx) is an adequate method to reduce the CO concentration to less than 10 ppm [1]. Thus, given the importance of the hydrogen purification process, the last few years have witnessed the surge of a renewed interest in the CO oxidation reaction, and several contributions dealing with this issue have recently been published.

A variety of catalyst formulations have been tested for the COPrOx reaction. Supported noble metals (Pt, Au) and the copper–ceria system are the most active and selective catalysts so far reported in the open literature [1]. Recently, other supported oxides have been investigated [2] as less expensive alternatives. Cobalt-containing catalysts have been the focus of numerous publications in the environmental catalysis field. Due to their redox properties, supported cobalt oxides have traditionally been studied for CO oxidation applications [3].

However, while most studies have been performed using powder catalysts, it is generally admitted that structured catalysts are necessary in this type of reactions for practical applications [4]. In this vein, the activity and stability of monolithic catalysts have been topics of recently published research work [5–7]. It is important to study the fundamentals of the structured catalysts since the interactions of the catalytic formulations with the materials of the monolithic supports can give rise to different behaviors if compared to the powder catalysts [8]. In this vein, Ayastuy et al. [6] reported interesting results using CuO/CeO_2 washcoated ceramic monoliths for COPrOx reaction. They used 7 wt.% and 9 wt.% of copper loading, the catalyst with lower loading being more active and selective in the absence of water and CO_2. However, CO_2 substantially inhibits the activity and selectivity of both monoliths, in particular 7% Cu loaded catalyst. H_2O also inhibits the activity and selectivity of both monoliths, although to a lower extent than that of CO_2. Arzamendi et al. [5] and Divins et al. [7] studied the performance of micro-structured catalysts (microreactors), using gold formulations (Au/CeFe and Au/TiO_2, respectively). In both contributions, it is concluded that microreactors constitute a promising technology to be employed in the COPrOx process, which is very exothermic and is characterized by a complex scheme of competing reactions in which heat transfer issues reach great relevance. However, a careful control of the reaction temperature is required in order to attain suitable oxygen selectivity to CO_2.

In previous studies [9,10], we reported results about the CO preferential oxidation over Co/ZrO_2 and Co/CeO_2 monolithic catalysts. The active formulations were those with Co loadings higher than 10 wt.% and showed Co_3O_4 as the main cobalt containing phase. In the case of Co/CeO_2, low Co loadings (below the solubility limit of cobalt in CeO_2) resulted in poor catalytic behavior, indicating that the segregation of Co_3O_4 is beneficial.

Preliminary studies with powder MnCoCe formulations with different Mn/Co molar ratios indicated that the catalyst with Mn/Co

* Corresponding author. Tel.: +54 342 4536861.
E-mail address: aboix@fiq.unl.edu.ar (A.V. Boix).

0920-5861/$ – see front matter © 2013 Elsevier B.V. All rights reserved.
http://dx.doi.org/10.1016/j.cattod.2013.05.010

ratio equal to 1/4 yielded the best activity results [11]. Thus, we selected this formulation to prepare monolithic catalysts.

In this work, we report new results on MnCoCe(CP) catalysts coated onto cordierite monoliths to be used in the COPrOx reaction. Activity and characterization results are compared with those obtained for structured catalysts based on Co/ZrO_2 and Co/CeO_2. The catalysts were characterized by Laser Raman Spectroscopy (LRS), X-ray Photoelectron Spectroscopy (XPS), X-ray Diffraction (XRD) and Scanning Electronic Microscopy (SEM). In the case of LRS and XRD characterizations, powder samples were also analyzed. This complementary characterization was carried out because the formation of a thin film covering the cordierite structure makes the concentration of the catalytic components relatively low. Thus, the intensity of the XRD and LRS signals became weaker, making it more difficult to interpret the results.

2. Experimental

2.1. Preparation of powder and monolithic catalysts

Cordierite honeycomb monoliths (Corning, 400 cpi, 0.1 mm wall thickness), $2MgO–2Al_2O_3–5SiO_2$, were used as substrates. The supports were cut in an average size of 1 cm × 1 cm and length 2 cm.

The MnCoCe/M monolith was prepared by washcoating of the MnCoCe(CP) catalyst which had been previously synthesized by co-precipitation of Mn, Co and Ce nitrates. Aqueous solutions of $Co(NO_3)_2·6H_2O$, $Ce(NO_3)_3·6H_2O$ and $Mn(NO_3)_2·4H_2O$ were simultaneously added into a continuously stirred flask in adequate amounts to get 10 wt.% of Co and a Mn/Co molar ratio of 1/4. An aqueous solution of $NH_4(OH)$ was added dropwise to the flask and then, the mixture was kept under continuous stirring for 2 h. The precipitate obtained was washed several times in deionized water, and then dried overnight at 110 °C. The resulting powder was calcined at 450 °C for 4 h under air flow. This powder was used to form an aqueous suspension, and then the bare cordierite pieces were immersed in this suspension successively in order to get an adequate catalytic layer thickness. After that, the prepared catalysts were calcined at 450 °C.

Both $Co(I)/ZrO_2$-M and $Co(I)/CeO_2$-M monoliths were prepared in a similar way, using suspensions of commercial powder ZrO_2 in acetic acid or CeO_2 in deionized water, respectively. The coatings were deposited onto cordierite by washcoating, immersing the monoliths during 30 s in 30 cm^3 of either a ZrO_2 or CeO_2 slurry. The whole cycle, immersion–drying–calcination (at 700 °C and 500 °C respectively, for 2 h in air) was repeated several times in order to achieve the desired loadings. The cobalt was incorporated by impregnation, immersing covered monoliths in a $Co(NO_3)_2$ aqueous solution.

The bare cordierite showed a surface area of 0.5 $m^2\,g^{-1}$. After washcoating, the BET area was between 1 and 2 $m^2\,g^{-1}$, depending on the catalyst loading. A summary of the catalysts preparation is shown in Table 1.

The adherence of catalyst films was evaluated using a method described in the patent literature [12]. The coated monoliths were subjected to ultrasound by immersing them in acetone inside a glass vessel and then in an ultrasonic bath, during 10 min (Cole Parmer, 47 kHz and 130 W). The weight of the sample both before and after the ultrasonic treatment was measured.

Powder catalysts with different combinations of Mn, Co, and Ce were also prepared by co-precipitation method in order to complement the characterization results obtained with monolithic catalysts. The CoCe(CP) powder was prepared with 10 wt.% Co in order to get the same charge as structured catalysts, while the MnCo(CP) powder was prepared with a Mn/Co molar ratio 1/4, in the same way as MnCoCe(CP).

2.2. Catalytic tests

Preferential CO oxidation experiments were performed in a fixed-bed flow reactor at atmospheric pressure. Monolithic samples were placed between quartz glass woods in a quartz reactor (17 mm diameter). In general, the reaction mixture consisted of CO 1%, O_2 1% and H_2 40%, He balance. The catalyst weight/total flow ratio was 2.1 mg cm^{-3} min. The CO conversion and selectivity toward CO_2 were defined as:

$$C_{CO} = \left(\frac{[CO]^\circ - [CO]}{[CO]^\circ}\right) \times 100$$

$$S = 0.5\left(\frac{[CO]^\circ - [CO]}{[O_2]^\circ - [O_2]}\right) \times 100$$

where [CO], $[O_2]$ are reactor exit concentrations and $[CO]^\circ$, $[O_2]^\circ$ represent feed concentrations, which were measured with a GC-2014 Shimadzu chromatograph equipped with a TCD cell. All the catalysts were pretreated during 1 h in oxygen flow at 200 °C before the catalytic test.

2.3. Catalysts characterization

2.3.1. Microscopic observations

The coatings of the monolithic samples were examined with a scanning electron microscope (SEM, JEOL JSM-35C operated at 20 kV) with the aim of studying their morphology. The samples were covered with a thin gold layer to improve the images. The images and the energy-dispersive X-ray spectroscopy (EDX) measurements were performed with an FEG-SEM Zeiss, SUPRA 40 with EDS detector (Oxford Instruments).

2.3.2. X-ray Diffraction (XRD)

The patterns of monolithic catalysts and powder samples were measured on a Shimadzu XD-D1 with monochromator using Cu Kα radiation at a scanning rate of 1° min^{-1} in 2θ = 20–80°. The peaks observed for the catalysts were compared to standards published by JCPDS (1995) data [13].

2.3.3. Laser Raman Spectroscopy (LRS)

The Raman spectra of calcined monoliths and powders were recorded using a LabRam spectrometer (Horiba-Jobin-Yvon) coupled to an Olympus confocal microscope (a 100× objective lens was used for simultaneous illumination and collection), equipped with a CCD detector cooled to about 200 K using the Peltier effect. The excitation wavelength was in all cases 532 nm (Spectra Physics diode pump solid state laser). The laser power was set at 30 mW.

2.3.4. X-ray Photoelectron Spectroscopy (XPS)

The surface features of the monolithic catalysts were studied in a multi-technique system (SPECS) equipped with a dual Mg/Al X-ray source and a hemispherical PHOIBOS 150 analyzer operating in the fixed analyzer transmission (FAT) mode. The spectra were obtained with pass energy of 30 eV, the Al Kα X-ray source was operated at 200 W and 12 kV. The working pressure in the analyzing chamber was less than 5.9×10^{-7} Pa. The XPS analyses were performed on the calcined samples. The MnCoCe/M monolith in situ reduced at 300 °C in the reaction chamber of the spectrometer was also analyzed. The spectral regions corresponding to Co 2p, O 1s, Ce 3d, Mn 2p, Zr 3p, Zr 3d and C 1s (reference B.E. 284.6 eV) core levels were recorded for each sample. The data treatment was performed with the Casa XPS program (Casa Software Ltda., UK). Peaks were considered to be a mixture of Gaussian and Lorentzian functions in a 70/30 ratio.

Please cite this article in press as: L.E. Gómez, et al., Co/ZrO_2, Co/CeO_2 and MnCoCe structured catalysts for COPrOx, Catal. Today (2013), http://dx.doi.org/10.1016/j.cattod.2013.05.010

Table 1
Characterization of monolithic catalysts.

Catalysts	Total weight gained (wt.%)[a]	Co (wt.%)	Weight loss[b] (%)	XRD phases
MnCoCe/M	10.9	10.0	2.6	CeO_2, Co_3O_4, $(Mn,Co)_3O_4$
Co(I)/CeO_2-M	12.0	11.0	1.7	Co_3O_4, CeO_2
Co(I)/ZrO_2-M	14.8	10.1	0.5	Co_3O_4, ZrO_2

[a] Over cordierite substrate.
[b] Calculated over structured catalyst.

3. Results and discussion

3.1. COPrOx on monolithic catalysts

The performance of monolithic catalysts in the COPrOx reaction was studied, in order to assess the behavior of the different formulations selected. Fig. 1 shows the curves for the conversion of CO (A) and the selectivity toward CO_2 (B) that corresponds to the three structured systems under study and the MnCoCe(CP) powder catalyst for comparison. Co(I)/ZrO_2-M is the least active catalyst, reaching a maximum conversion of 87% at 250 °C. The Co(I)/CeO_2-M catalyst has a better performance, showing a CO conversion curve with a maximum at 200 °C, where C_{CO} is almost complete (98%). When the active phase is prepared by the co-precipitation method (MnCoCe/M), the CO conversion curve shifts to lower temperatures. For this catalyst, 95% of CO conversion occurs at 190 °C and then, the curve shows the same trend as the other two catalysts. Furthermore, for a low reaction temperature, the conversion reached by the MnCoCe/M catalyst is higher than those of the Co(I)/CeO_2-M and Co(I)/ZrO_2-M catalysts.

With regard to the selectivity curves, an important difference can be noticed for the three catalysts. While Co(I)/ZrO_2-M and MnCoCe/M show a maximum of 86% and 77% at 130 °C and 176 °C, respectively, the Co(I)/CeO_2-M curve shows 100% selectivity at lower temperature and then decreases when the temperature increases. On the other hand, as said in the previous paragraph, among the monolithic catalysts studied here, the best CO conversion is reached for the MnCoCe/M structured catalyst. However, the oxygen selectivity to CO_2 is lower as compared with the unpromoted Co(I)/CeO_2-M, suggesting that the improvement in the redox behavior due to the presence of Mn increases not only the CO oxidation rate but also the oxidation of hydrogen.

Another important result about the features of the MnCoCe/M structured system is the comparison with the powder formulation. Fig. 1 shows that catalytic experiments performed with the powder MnCoCe(CP) yields a slightly better performance in terms of CO conversion, indicating that some mass transfer limitations could occur in the catalytic layer coated on the monolith.

3.2. Characterization of monoliths and powder samples

In order to better understand the catalytic behavior of the catalysts, and to gain insight about the influence of the monolithic structure, different characterization techniques were used. Fig. 2 shows SEM pictures of the three monolithic catalysts studied. The surface morphology of the cordierite coated with the catalysts reveals that in all cases, the active films are constituted of polydispersed, non-uniform particles. The catalytic film is homogeneously distributed, so that the macroporosity of the cordierite is completely blocked. As it can be observed on the right of each figure, the incorporated catalytic particles are well adhered to the cordierite support.

The weight gain of the different monoliths washcoated with the active catalysts varies between 10 and 15 wt.% (Table 1). Likewise, in all samples, the amount of loaded cobalt was around 10–11 wt.% (referred to the coating weight). The compact structure of the catalytic coatings that is evident through the SEM observations, could be the cause of the slightly lower CO conversions obtained as compared with the MnCoCe powder. As a matter of fact, the slower mass transfer process across the catalytic film could pose a limitation to the access of CO and O_2 molecules to the active sites.

Fig. 3 presents XRD patterns of monolithic catalysts MnCoCe/M, Co(I)/ZrO_2-M and Co(I)/CeO_2-M and reference compounds (pure

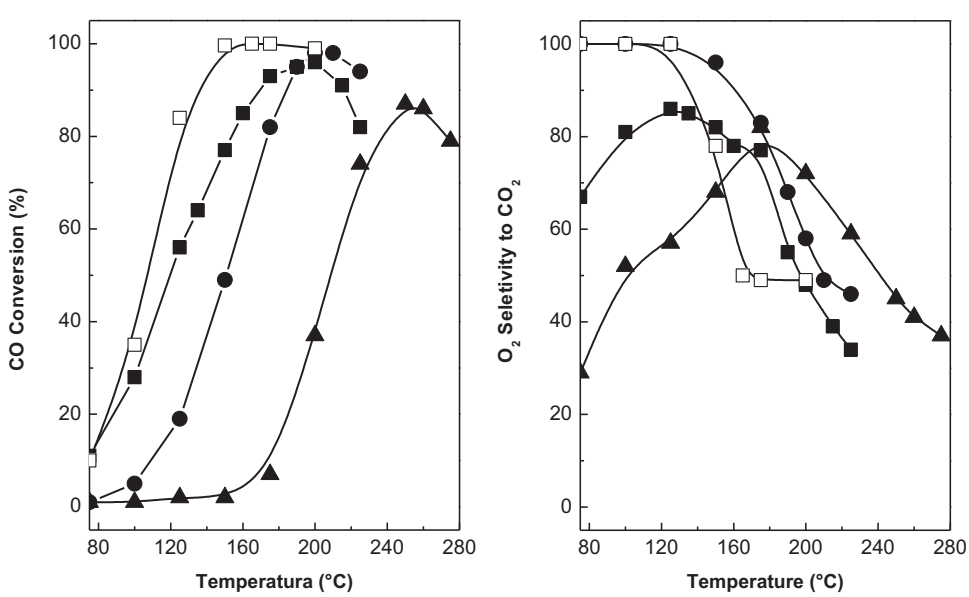

Fig. 1. COPrOx reaction on monolithic catalysts. (A) CO conversion (%). (B) O_2 selectivity to CO_2 (%). ■MnCoCe/M, ●Co(I)/CeO_2-M, ▲Co(I)/ZrO_2-M and □MnCoCe(CP) powder. Reaction conditions: CO 1%, O_2 1%, H_2 40%, He. W/F: 2.1 mg cm^{-3} min.

Please cite this article in press as: L.E. Gómez, et al., Co/ZrO_2, Co/CeO_2 and MnCoCe structured catalysts for COPrOx, Catal. Today (2013), http://dx.doi.org/10.1016/j.cattod.2013.05.010

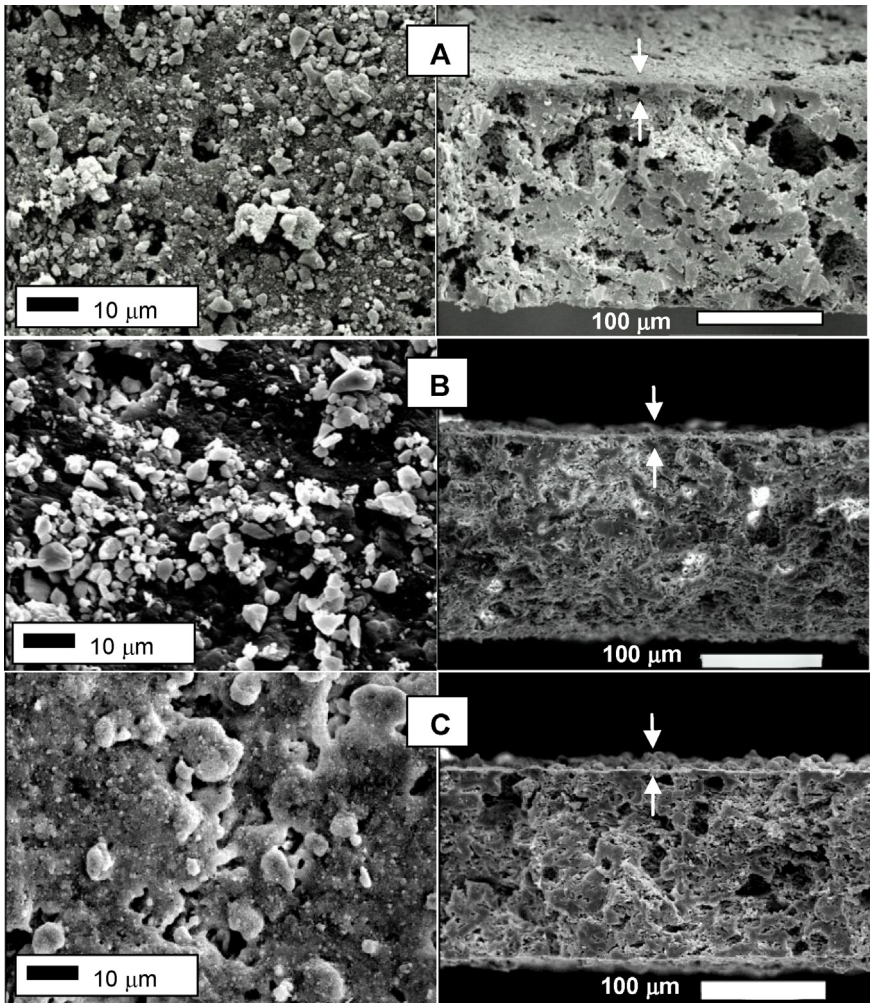

Fig. 2. SEM micrographs of cordierite coated with (A) MnCoCe/M, (B) Co(I)/CeO_2-M and (C) Co(I)/ZrO_2-M. Right side: top view. Left side: cross-section view.

monoclinic ZrO_2 and CeO_2). All diffractograms of monolithic catalysts mainly exhibit the signals associated with the cordierite patterns at $2\theta = 29.5°$, 28.5°, 21.7°, 26.4° and 33.9° (JCPDS 82-1844). The Co(I)/ZrO_2-M shows the peaks associated with the monoclinic ZrO_2 at $2\theta = 28.4°$, 31.5°, 33.9°, 35.3° and 24.0° (JCPDS 80-966), and the Co(I)/CeO_2-M diffractogram depicts the signal corresponding to CeO_2 at $2\theta = 33.1°$ and $2\theta = 28.6°$ (overlapped with a cordierite peak). In these two structured catalysts, the main peak of Co_3O_4 is detected at $2\theta = 36.8°$ (JCPDS 42-1467), although it could be overlapped with a cordierite diffraction peak.

The MnCoCe/M diffraction pattern shows a peak at $2\theta = 36.4°$ and an asymmetry detected in the peak at 29.5°, assigned to the mixed spinel $(Mn,Co)_3O_4$ (JCPDS 18-408). A weak signal at 36.8° might indicate the presence of the Co_3O_4 phase. However, the overlap with the cordierite pattern makes it difficult to identify different species.

Powder samples, with different formulations, were also characterized in order to better interpret the results obtained for the MnCoCe/M monolithic catalyst. Fig. 4 shows the XRD patterns of different combinations of Co, Mn and Ce (CoCe(CP), MnCo(CP) and MnCoCe(CP)).

The most important peaks in the CoCe(CP) diffractogram correspond to CeO_2 ($2\theta = 28.6°$, 33.4°, 47.8° and 56.6°) and Co_3O_4 ($2\theta = 31.3°$, 36.8°, 44.8°, 59.4° and 65.3°) phases (JCPDS 34-0394 and JCPDS 42-1467, respectively). In the MnCo(CP) sample, no signals of manganese oxides are observed, only diffraction peaks associated with Co_3O_4 are detected.

The diffraction pattern of the powder MnCoCe(CP) sample shows a broadening of peaks corresponding to the CeO_2 phase. These results could indicate that the structure of CeO_2 is distorted due to the insertion of manganese, although the type-fluorite structure of CeO_2 is still maintained [14]. Also, the main peak of the $(Mn,Co)_3O_4$ phase ($2\theta = 36.4°$) appears in this sample at 36.9°, close to the main signal of the Co_3O_4 spinel.

Similar formulations of the CoMnCe system prepared with different proportions of the constituent elements have shown the coexistence of two phases, Co_3O_4 and CeO_2 [15,16]. On the other hand, many other studies have demonstrated the formation of the $Mn_xCo_{3-x}O_4$ solid solution in the Mn-Co-O binary oxide [17].

The average size of crystals in powder samples resulted between 5 and 20 nm. These were calculated using Scherrer's equation, considering the main peaks in each diffractogram [18].

The monolithic catalysts were also characterized by Laser Raman Spectroscopy, and the spectra are shown in Fig. 5. In the MnCoCe/M spectrum, a broad peak at 455 cm^{-1} might be assigned to CeO_2 [19,20]. Weak signals at 184, 511, 615 and 688 cm^{-1} are attributed to the Co_3O_4 spinel [19,21], but the simultaneous presence of Mn_3O_4 with a strong signal at 640–660 cm^{-1} could not be discarded [22–24]. The active Raman vibration corresponding to Co_3O_4 is well defined in the Co(I)/CeO_2-M and Co(I)/ZrO_2-M monoliths due to the absence of manganese. A mostly monoclinic zirconia phase is detected for the Co(I)/ZrO_2-M catalyst [25], while a small peak at 466 cm^{-1} corresponding to CeO_2 is detected in the Co(I)/CeO_2-M spectrum.

Please cite this article in press as: L.E. Gómez, et al., Co/ZrO_2, Co/CeO_2 and MnCoCe structured catalysts for COPrOx, Catal. Today (2013), http://dx.doi.org/10.1016/j.cattod.2013.05.010

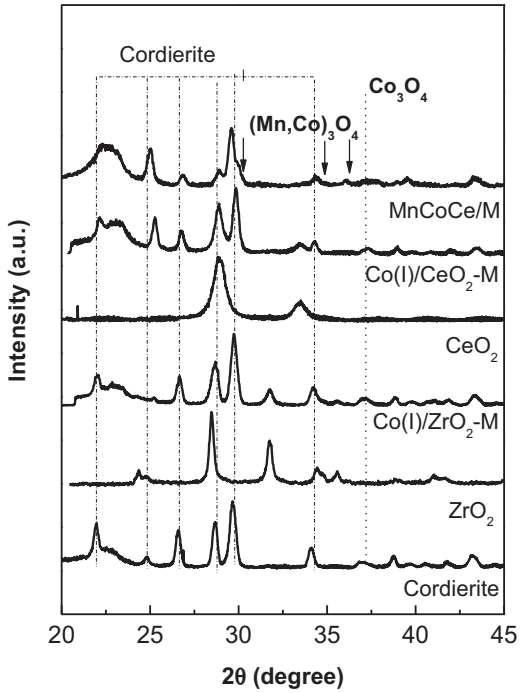

Fig. 3. XRD diffractograms of the monolithic catalysts as well as CeO_2, ZrO_2 and cordierite monolith.

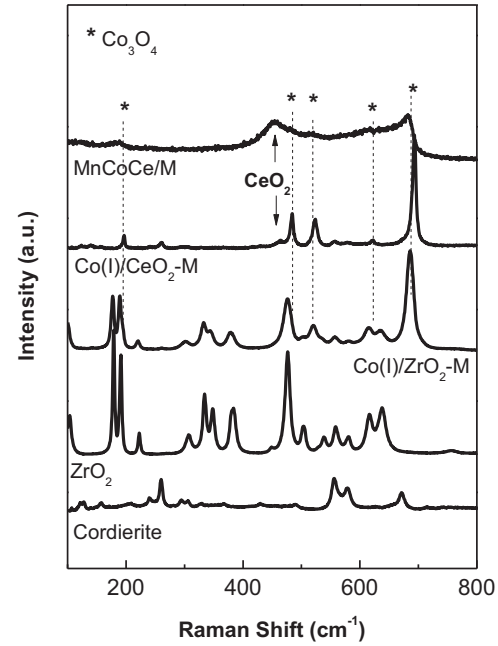

Fig. 5. L. Raman spectra of structured catalysts, ZrO_2 powder and cordierite.

Fig. 6 shows LRS spectra of the different powder combinations of Co, Mn and Ce composites. The bicomponent CoCe(CP) spectrum clearly shows the five Raman-activated modes of pure Co_3O_4 at 197, 480, 521, 618 and 689 cm^{-1} [19,21], as well as a peak at 463 cm^{-1} which corresponds to CeO_2. The MnCo(CP) spectrum shows two broad signals and a small peak at 178 cm^{-1} in the 400–700 cm^{-1} range. The signal between 550 and 700 cm^{-1} seems to be composed of two peaks, which might correspond to the main signals of Mn_3O_4 and Co_3O_4. The spectrum of powder MnCoCe(CP) shows a widening and a slight shift to a lower wave-number in the peak associated with CeO_2. This effect might be related to the introduction of Mn in the CeO_2 structure, as reported by Hong et al. [22]. In this spectrum, two broad and weak signals are centered at 590 cm^{-1} and 660 cm^{-1} and they are associated with Mn_3O_4 species [22–24]. In addition, a substitution of Co ions by Mn ions to form a mixed $(Mn,Co)_3O_4$ phase might also be considered. This is a difference compared with the LRS spectrum of the structured sample, in which the Co_3O_4 species are clearly detected. This result could indicate a different behavior when the powder catalyst is washcoated on the monolith, probably due to interactions with the cordierite surface.

Thus, from the point of view of the crystalline structures as seen by XRD, together with LRS results, it is concluded that similar phases are present in both powder and monolithic MnCoCe

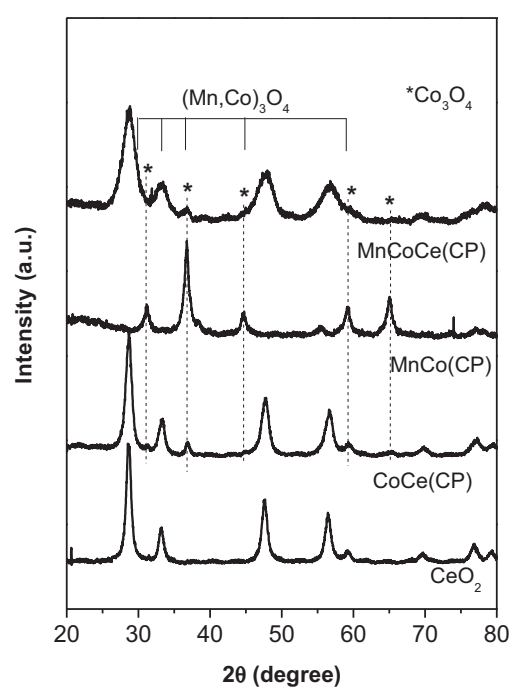

Fig. 4. XRD diffractograms of powder samples prepared by co-precipitation.

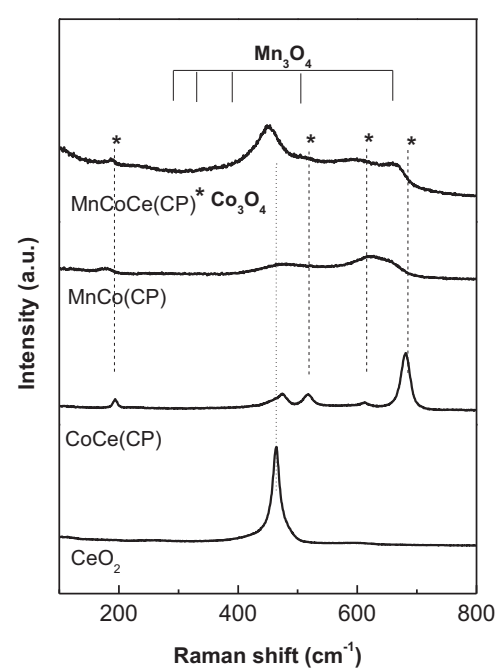

Fig. 6. L. Raman spectra of powder prepared by co-precipitation.

Please cite this article in press as: L.E. Gómez, et al., Co/ZrO_2, Co/CeO_2 and MnCoCe structured catalysts for COPrOx, Catal. Today (2013), http://dx.doi.org/10.1016/j.cattod.2013.05.010

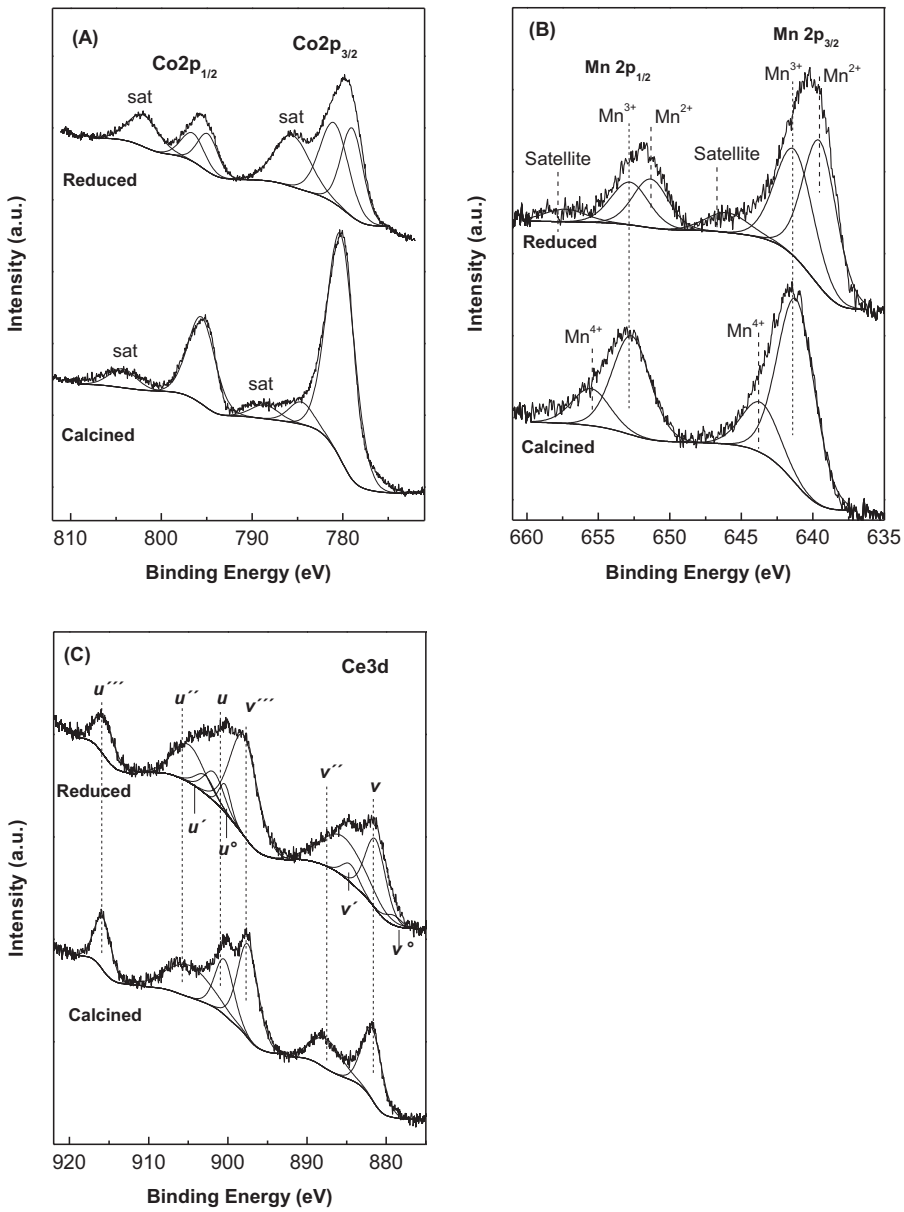

Fig. 7. XPS spectra of MnCoCe/M monolith calcined and reduced in situ (300 °C).

catalysts. The only difference observed is the poor definition of LRS signals corresponding to Co_3O_4 species for monolithic catalysts. This is an important fact, because it shows that we were able to deposit the active phases obtained in the powder formulations on the monolithic structure, the small change in catalytic properties being ascribed to physical reasons (mass transfer limitations) and to some small differences in the structure of the Co_3O_4 active phase.

Since not only the chemical structure of the catalytic solids is important, but also the species present on the surface, XPS measurements were conducted for the calcined monolithic catalyst MnCoCe/M. In addition, since the reaction atmosphere is rich in hydrogen, we also analyzed the sample reduced in situ at 300 °C by H_2/Ar flow.

The spectra of the Co 2p region are shown in Fig. 7A. The main peak of Co $2p_{3/2}$ of the calcined catalyst at 780.3 ± 0.1 eV (fwhm = 3.6 eV) can be observed as well as the satellite peaks at higher binding energy, with a spin-orbit doublet $Co2p_{1/2}$–$Co2p_{3/2}$ about 15.0 eV (Table 2). Even though the BE values of Co^{3+} and Co^{2+} are relatively close, both oxidation states of cobalt can be distinguished by the presence of a distinct shake-up satellite structure in Co^{2+}, arising from the presence of unpaired electrons in the valence orbital. Co^{3+} is almost always in a low spin state and, therefore, there can be no energy transfer to an unpaired electron, meaning that a shake-up satellite structure is not observed [26,27]. In the calcined monolith, the satellite intensity is relatively low and the ratio to the main peak (I_{sat}/I_{main}) is 0.14, which indicates that Co^{3+} is the predominant species on the surface [28]. Moreover, the Co 2p spectrum of the reduced catalyst shows the contribution of two components at 779.0 and 781.0 eV and the significant increase of satellite peaks ($I_{sat}/I_{main} = 0.43$) due to presence of Co^{2+} on the surface (Table 2).

The manganese $2p_{3/2-1/2}$ region (Fig. 7B) was also studied on the calcined monolith and a mix of Mn^{4+} (BE = 643.6 eV) and Mn^{3+} (BE = 641.2 eV) components was detected on the catalytic surface (Table 2), in agreement with XPS data published by other authors [29]. The spin-orbital splitting $2p_{3/2}$–$2p_{1/2}$ measured were 11.5 eV (Mn^{3+}) and 11.9 eV (Mn^{4+}). Gautier et al. [30] studied $Mn_xCo_{3-x}O_4$ compounds and reported similar values.

Table 2
XPS Data of monolythic catalysts.

Catalyst	BE Co2p$_{3/2}$ (fwhm), eV	I_{sat}/I_{main} Co2p$_{3/2}$	BE Mn 2p$_{3/2}$ (fwhm), eV	Molar surface ratio[a]	
				Mn/Co	Co/Ce or Co/Zr
MnCoCe/M	780.3 (3.6)	0.14	641.2 (3.1) 77% 643.6 (3.1)	0.46 (0.25)	3.9 (1.0)
MnCoCe/M (reduced)	779.0 (2.9) 46% 781.0 (3.7)	0.43	639.5 (2.8) 41% 641.3 (3.1)	0.29 (0.25)	4.7 (1.0)
Co(I)/CeO_2-M	780.0 (3.7)	0.25	–	–	0.4 (0.14)
Co(I)/ZrO_2-M	780.2 (3.5)	0.25	–	–	0.6 (0.18)

[a] Molar bulk ratio between parentheses.

After reduction, the peaks were shifted to the lower binding energy region (Fig. 7B). The signals of Mn 2p$_{3/2}$ at 639.5 and 641.3 eV corresponded to Mn^{2+} and Mn^{3+} species, respectively [31,32]. In addition, a satellite peak was observed at 646.0 eV characteristic of the presence of Mn^{2+} [29,33,34].

Finally, Fig. 7C shows the Ce 3d spectral region. In the calcined monolith only Ce^{4+} species are observed. The spectrum is fitted with six peaks whose binding-energy positions are very close to those found in the CeO_2 sample. As mentioned by several authors [35–37], the CeO_2 spectrum is composed of several peaks; each component of the spin-orbit split doublet (usually referred to as v and u and associated with Ce 3d$_{5/2}$ and Ce 3d$_{3/2}$, respectively) contains three peaks. The lower binding energy peaks at 881.8, 887.6 and 897.5 eV, which correspond to the v, v'' and v''' peaks, are characteristic of Ce 3d$_{5/2}$, while the other three peaks, u, u'' and u''', located at 900.5, 904.9 and 915.8 eV, respectively are assigned to Ce 3d$_{3/2}$. When the catalysts is reduced with a H_2/Ar flow at 300 °C in the pretreatment chamber of the spectrometer, there appear four additional peaks associated with Ce^{3+} species (Fig. 7C).

The O1s XP spectra can be described as the result of the overlapping of two components around 529.3 and 531.4 eV. The first one corresponds to the surface lattice oxygen of oxides, and the other peak at higher BE is associated with surface oxygen ions with low coordination, which are ascribed to the presence of hydroxyl and/or water adsorbed on the material surface [38].

The surfaces of calcined Co(I)/ZrO_2-M and Co(I)/CeO_2-M monolithic catalysts were also analyzed. The XPS signal in the Co2p region consisted of two main peaks about 780.0 ± 0.1 eV, Co 2p$_{3/2}$, and at 795.0 eV, Co 2p$_{1/2}$, with their corresponding weak satellite peaks at higher binding energies (Table 2). The main peaks are the contribution of Co^{2+} and Co^{3+} species present in Co_3O_4 ($Co^{2+}2Co^{3+}O_4$) [9,10,28].

Table 2 shows the surface ratios of Mn, Co and Ce present in the monolithic catalyst. It can be seen that for the calcined sample, the surface Mn/Co ratio is 0.46, which is higher than the bulk value (Mn/Co = 0.25). We also analyzed the reduced sample, and the surface Mn/Co ratio decreased to 0.29, value closer to the bulk metal content. Moreover, cobalt surface enrichment was detected in all monolithic catalysts.

After an analysis of characterization results, it is concluded that, even though Co_3O_4 was present in all catalysts and indicated as the active species in the COPrOx reaction, Co(I)/CeO_2-M and MnCoCe/M catalysts resulted more active than Co(I)/ZrO_2-M, possibly due to the better redox properties of the ceria. CeO_2 has a high capacity to store and release oxygen which allows it to move surface oxygen species easily compared with conventional oxides such as SiO_2, Al_2O_3, MgO and ZrO_2 [39]. In addition, in the MnCoCe/M catalyst prepared by the co-precipitation method, the addition of Mn represents a positive effect. The presence of Mn promotes the re-oxidation of Co^{2+} to Co^{3+} and, consequently, the activity increases at low temperature. In agreement with our results, Guo and Liu [16] also reported that the MnOx addition to Co_3O_4–CeO_2 exhibited much better catalytic performance for COPrOx at low temperature and exhibited a broad temperature window for complete CO conversion.

4. Conclusions

A cordierite monolith washcoated with the MnCoCe(CP) catalyst constitutes an attractive system to be further explored for its application in the COPrOx reaction. The said catalyst presented higher CO conversion at lower temperatures as compared with Co(I)/ZrO_2 Co(I)/CeO_2-M catalysts also coated on monoliths. However, the selectivity toward CO_2 was somewhat better for the Co(I)/CeO_2-M catalyst. The Ce-containing catalysts are more active than Co(I)/ZrO_2-M catalysts because ceria promotes the efficiency of the cobalt redox couple. In addition, the intimate contact between Mn, Co and Ce species on the monolith surface improves the catalytic activity.

The XRD and LRS characterization showed that the Co_3O_4 active phase is present in all structured catalysts and the cobalt surface enrichment was observed by XPS.

The methods used in this work for the preparation of the monolithic catalysts consisted in the conventional washcoating process using different suspension formulations. It has been shown that homogeneous and mechanically stable coatings were obtained which in turn yielded promising results in the COPrOx reaction. While the interaction between the oxide mixtures and the cordierite support resulted in some alterations of the species distribution as seen by LRS, the catalytic behavior was only slightly altered. This is an important fact, because it shows that we were able to deposit the active phases obtained in the powder formulations on the monolithic structure, the small decrease in catalytic activity being ascribed to physical reasons (mass transfer limitations) and to some small differences in the structure of the Co_3O_4 active phase.

The effect of carbon dioxide, water, and time-on-stream will be considered in further studies.

Acknowledgments

The authors acknowledge the financial support received from UNL, CONICET and ANPCyT. They are grateful to ANPCyT for the purchase of the SPECS multitechnique analysis instrument (PME 8-2003). Thanks are given to Fernanda Mori for the XPS measurements and to Elsa Grimaldi for the English language editing.

References

[1] N. Bion, F. Epron, M. Moreno, F. Mariño, D. Duprez, Topics in Catalysis 51 (2008) 76–88.
[2] A. Firsova, T. Khomenko, O. Silchenkova, V. Korchak, Kinetics and Catalysis 51 (2) (2010) 299–311.
[3] P. Thormählen, M. Skoglundh, E. Fridell, B. Andersson, Journal of Catalysis 188 (2) (1999) 300–310.
[4] P. Avila, M. Montes, E.E. Miró, Chemical Engineering Journal 109 (2005) 11–36.

[5] G. Arzamendi, I. Uriz, P.M. Dieguez, O.H. Laguna, W.Y. Hernandez, A. Alvarez, M.A. Centeno, J.A. Odriozolab, M. Montesc, L.M. Gandia, Chemical Engineering Journal 167 (2011) 588–596.
[6] J.L. Ayastuy, N.K. Gamboa, M.P. Gonzalez-Marcos, M.A. Gutierrez-Ortiz, Chemical Engineering Journal 171 (2011) 224–231.
[7] N.J. Divins, E. Lopez, M. Roig, T. Trifonov, A. Rodrıguez, F. Gonzalez de Rivera, L.I. Rodríguez, M. Seco, O. Rossell, J. Llorca, Chemical Engineering Journal 167 (2011) 597–602.
[8] A.V. Boix, J.M. Zamaro, E.A. Lombardo, E.E. Miró, Applied Catalysis B 46 (2003) 121–132.
[9] L.E. Gómez, I.S. Tiscornia, A.V. Boix, E.E. Miró, Applied Catalysis A 401 (2011) 124–133.
[10] L.E. Gómez, I.S. Tiscornia, A.V. Boix, E.E. Miró, International Journal of Hydrogen Energy 37 (2012) 14812–14819.
[11] L.E. Gómez, E.E. Miró, A.V. Boix, International Journal of Hydrogen Energy 38 (2013) 5645–5654.
[12] S. Yasaki, Y. Yoshino, K. Ihara, K. Ohkubo, US Patent 5,208,206 (1993).
[13] Joint Committee on Powder Diffraction Standards, 1995.
[14] G. Picasso, M. Gutiérrez, M.P. Pina, J. Herguido, Chemical Engineering Journal 126 (2007) 119–130.
[15] Z. Zhao, R. Jin, T. Bao, H. Yang, X. Lin, G. Wang, International Journal of Hydrogen Energy 37 (2012) 4774–4786.
[16] Q. Guo, Y. Liu, Applied Catalysis B 82 (2008) 19–26.
[17] Q. Zhang, X. Liu, W. Fan, Y. Wang, Applied Catalysis B 102 (2011) 207–214.
[18] C. Ryul Jung, A. Kundu, S. Woo Nam, H. Lee, Applied Catalysis A 331 (2007) 112–120.
[19] M.P. Wood, P. Gawade, B. Tan, U. Ozkan, Applied Catalysis B 97 (2010) 28–35.
[20] J. Xu, P. Li, X. Song, C. He, J. Yu, Y.F. Han, Journal of Physical Chemistry Letters 1 (2010) 1648–1654.
[21] A. Alvarez, S. Ivanova, M.A. Centeno, J.A. Odriozola, Applied Catalysis A 431–432 (2012) 9–17.
[22] W.J. Hong, S. Iwamoto, S. Hosokawa, K. Wada, H. Kanai, M. Inoue, Journal of Catalysis 277 (2011) 208–216.
[23] T. Gao, H. Fjellvåg, P. Norby, Analytica Chimica Acta 648 (2009) 235–239.
[24] Y.F. Han, F. Chen, Z. Zhong, K. Ramesh, L. Chen, E. Widjaja, Journal of Physical Chemistry B 110 (2006) 24450–24456.
[25] L.K. Noda, N.S. Goncalves, S.M. de Borba, J.A. Silveira, Vibrational Spectroscopy 44 (2007) 101–107.
[26] H.A.E. Hagelin-Weaver, G.B. Hoflund, D.M. Minahan, G.N. Salaita, Applied Surface Science 235 (2004) 420–448.
[27] L.F. Liotta, G. Di Carlo, G. Pantaleo, A.M. Venezia, G. Deganello, Applied Catalysis B 66 (2006) 217–227.
[28] D. Pietrogiacomi, M.C. Campa, S. Tuti, V. Indovina, Applied Catalysis B 41 (2003) 301–312.
[29] S. Ardizzone, C.L. Bianchi, D. Tirelli, Colloids and Surfaces A 134 (1998) 305–312.
[30] J.L. Gautier, E. Rios, M. Gracia, J.F. Marco, J.R. Gancedo, Thin Solid Films 311 (1997) 51–57.
[31] Z.Q. Zou, M. Meng, Y.Q. Zha, Journal of Physical Chemistry C 114 (2010) 468–477.
[32] F. Wang, H. Dai, J. Deng, G. Bai, K. Ji, Y. Liu, Environmental Science and Technology 46 (2012) 4034–4041.
[33] G.A. Rizzi, R. Zanoni, S. Di Siro, L. Perriello, G. Granozzi, Surface Science 462 (2000) 187–194.
[34] I. Olefjord, X-ray photoelectron spectroscopy, in: D. Brune, R. Hellborg, H.J. Whitlow, O. Hunderi (Eds.), Surface Characterization. A User's Sourcebook, Wiley VCH, Weinheim, 1997, pp. 291–319.
[35] F. Le Normand, L. Hilaire, K. Kili, G. Krill, G. Mairet, Journal of Physical Chemistry 92 (1988) 2561–2568.
[36] F. Larachi, J. Pierre, A. Adnot, A. Bernis, Applied Surface Science 195 (2002) 236–250.
[37] J. Swiatowska, V. Lair, C. Pereira-Nabais, G. Cote, P. Marcus, A. Chagnes, Applied Surface Science 257 (2011) 9110–9119.
[38] M. Alvarez, T. López, J.A. Odriozola, M.A. Centeno, M.I. Domínguez, M. Montes, P. Quintana, D.H. Aguilar, R.D. González, Applied Catalysis B 73 (2007) 34–41.
[39] G. Ranga Rao, B.G. Mishra, Bulletin of the Catalysis Society of India 2 (2003) 122–134.

Please cite this article in press as: L.E. Gómez, et al., Co/ZrO_2, Co/CeO_2 and MnCoCe structured catalysts for COPrOx, Catal. Today (2013), http://dx.doi.org/10.1016/j.cattod.2013.05.010